Journal of
Composites Science

MDPI

Article

Micro and Macro Analyses for Structural, Mechanical, and Biodegradability of a Pulp-Based Packaging Material: A Comprehensive Evaluation Using SEM, XRD, FTIR, and Mechanical Testing

H. M. D. U. Sewwandi [1,2,3], J. D. Chathuranga [2], W. G. C. M. Kulasooriya [2], D. K. A. Induranga [2,3], S. V. A. A. Indupama [2,3,4], G. D. C. P. Galpaya [2,3], M. K. D. M. Gunasena [3,5], H. V. V. Priyadarshana [2,3,4] and K. R. Koswattage [2,3,*]

1 Department of Materials Science and Engineering, Faculty of Engineering, University of Moratuwa, Moratuwa 10400, Sri Lanka; sewwandihmdu.24@uom.lk
2 Department of Engineering Technology, Faculty of Technology, Sabaragamuwa University of Sri Lanka, Belihuloya 70140, Sri Lanka; dileepachathuranga23@gmail.com (J.D.C.); cmkulasooriya@gmail.com (W.G.C.M.K.); ashaninduranga@tech.sab.ac.lk (D.K.A.I.); amalka@tech.sab.ac.lk (S.V.A.A.I.); chanakagalpaya@gmail.com (G.D.C.P.G.); vimukkthi@tech.sab.ac.lk (H.V.V.P.)
3 Center for Nano Device Fabrication and Characterization (CNFC), Faculty of Technology, Sabaragamuwa University of Sri Lanka, Belihuloya 70140, Sri Lanka; kasundi@tech.sab.ac.lk
4 Faculty of Graduate Studies, Sabaragamuwa University of Sri Lanka, Belihuloya 70140, Sri Lanka
5 Department of Bio Systems Technology, Faculty of Technology, Sabaragamuwa University of Sri Lanka, Belihuloya 70140, Sri Lanka
* Correspondence: koswattagekr@appsc.sab.ac.lk; Tel.: +94-704-565-000

check for updates

Academic Editor: José António Covas

Received: 6 June 2025
Revised: 4 July 2025
Accepted: 7 July 2025
Published: 14 July 2025

Citation: Sewwandi, H.M.D.U.; Chathuranga, J.D.; Kulasooriya, W.G.C.M.; Induranga, D.K.A.; Indupama, S.V.A.A.; Galpaya, G.D.C.P.; Gunasena, M.K.D.M.; Priyadarshana, H.V.V.; Koswattage, K.R. Micro and Macro Analyses for Structural, Mechanical, and Biodegradability of a Pulp-Based Packaging Material: A Comprehensive Evaluation Using SEM, XRD, FTIR, and Mechanical Testing. *J. Compos. Sci.* **2025**, *9*, 365. https://doi.org/10.3390/jcs9070365

Copyright: © 2025 by the authors. Licensee MDPI, Basel, Switzerland. This article is an open access article distributed under the terms and conditions of the Creative Commons Attribution (CC BY) license (https://creativecommons.org/licenses/by/4.0/).

Abstract

The extensive accumulation of plastic waste causes serious environmental problems, leading to growing interest in biodegradable alternatives. In this study, the structural, chemical, and crystalline characteristics of a pulp-based material incorporating sugarcane bagasse ash (SCBA) were investigated using Scanning Electron Microscopy (SEM), X-ray Diffraction (XRD), and Fourier Transform Infrared Spectroscopy (FTIR). Mechanical properties of the materials were investigated through compression, tensile, and bending tests in order to assess their strength and flexibility, while biodegradability was evaluated through soil burial tests. The results indicate that SCBA addition enhances compressive strength, with optimal performance obtained at 15% SCBA content, while tensile and bending strengths showed an enhancement at 5% content. FTIR and XRD analyses suggested an increase in amorphous regions and notable microstructural interactions between SCBA particles and cellulose fibers, particularly at a 10% concentration. SEM images further confirmed effective particle dispersion and improved porosity in the composite materials. Furthermore, samples incorporating SCBA exhibited superior biodegradability compared to pure pulp. Overall, these findings highlight that incorporating 10–15% SCBA provides a promising balance between mechanical integrity and environmental sustainability, offering a viable strategy for developing eco-friendly, high-performance packaging materials.

Keywords: sugarcane bagasse ash; biodegradable composites; agricultural waste valorization; sustainable packaging; biodegradability

1. Introduction

The increasing accumulation of plastic waste has led to severe environmental degradation, prompting a global shift toward sustainable alternatives in various industries, particularly packaging [1]. Conventional petroleum-based plastics, although widely used due to their durability and low cost, pose significant challenges due to their non-biodegradability and long-term persistence in ecosystems [2]. In response, biodegradable materials derived from renewable resources have gained considerable attention, especially those based on lignocellulosic biomass, which offers biodegradability, mechanical strength, and abundant availability [3].

Sugarcane bagasse (SCB), a fibrous residue generated during sugar production, has emerged as a promising feedstock for sustainable materials. Globally, millions of tons of SCB are produced annually, yet much of it is utilized solely for energy generation through combustion [4]. Recent advancements have demonstrated the feasibility of converting SCB into value-added products such as cellulose nanofibers, microcrystalline cellulose, and biodegradable films [5], highlighting its potential beyond traditional applications.

A novel approach to further utilize SCB involves the incorporation of SCBA as a functional additive in biodegradable composites. SCBA, obtained by burning SCB at high temperatures, contains significant amounts of amorphous silica and other minerals, making it a candidate for reinforcing pulp-based matrices [6]. Despite its widespread use in construction and soil amendment, SCBA remains underexplored in the context of biodegradable packaging materials, especially when combined with pulp fibers [7].

Numerous studies have explored the use of natural fillers such as rice husk ash, lignin, and nanoclay in biopolymer matrices, showing that these additives can significantly improve mechanical properties and accelerate biodegradation [8]. Particle size, surface chemistry, and dispersion methods have been identified as critical factors influencing filler-matrix interactions and overall composite performance [5]. However, most of these studies focus on synthetic polymer systems, leaving a notable gap in the understanding of how SCBA interacts with lignocellulosic pulp matrices [9].

Biodegradable packaging materials face inherent trade-offs between mechanical strength, moisture resistance, and environmental degradability. While natural fiber-based materials offer eco-friendliness, they often exhibit inferior mechanical performance compared to synthetic counterparts [10]. To overcome this limitation, researchers have explored the integration of natural fillers that enhance structural integrity without compromising sustainability [11]. For instance, bacterial cellulose composites reinforced with curcumin and chitosan have shown promise in food packaging due to their antimicrobial properties and biodegradability [12]. Similarly, starch-based foams reinforced with grape stalks have demonstrated potential as protective packaging materials [13].

Despite these advances, few studies have systematically evaluated the impact of SCBA on the structural, chemical, and biodegradability characteristics of pulp-based composites. Existing research lacks comprehensive analysis of crystallinity changes, interfacial bonding, and microstructural effects resulting from SCBA incorporation [14–18]. This absence of detailed investigations presents a clear knowledge gap, justifying the need for a thorough evaluation of SCBA's role in enhancing both mechanical and environmental performance in pulp-based packaging. Therefore, these properties still require further enhancement without compromising each other to be viable for use in sustainable packaging applications.

This study addresses this gap by investigating the influence of SCBA content (0–20%) on the structural, mechanical, and biodegradability properties of pulp-based composites using advanced analytical techniques including SEM, XRD, FTIR, and mechanical testing. The objective was to determine the optimal SCBA concentration that balances mechanical

enhancement with environmental degradation, contributing to the development of high-performance, eco-friendly packaging materials.

These results establish SCBA as a promising, underutilized resource for sustainable packaging, offering a viable pathway to repurpose industrial agricultural waste into functional, biodegradable materials. By providing a multi-scale understanding of SCBA-pulp interactions, this work contributes to the broader effort of developing green packaging solutions aligned with circular economy principles.

2. Materials and Methods

The samples were prepared to analyze the effect of SCBA as the natural strengthening additive in both micro and macro ways, according to the following standard sample sizes (Table 1).

Table 1. Sample preparation details for various test methods.

Test Method	Sample Shape	Size
SEM		
FTIR	Thin film	10 mm × 10 mm × 1 mm
XRD		20 mm × 20 mm × 1 mm
Biodegradability		
Tensile test	Thin sheet	250 mm × 25 mm × 1 mm
Compression test	Cylindrical	55 mm × 50 mm
Bending test	Paper plate	80 mm × 25 mm × 0.8 mm

To analyze the strengthening effect, all the samples were prepared following the exact same mass manufacturing method. The following raw materials were used for preparing the samples.

- Sugarcane bagasse ash: Fly ash was collected from Ethimale Plantation (Pvt) Ltd., located in the Monaragala district of Sri Lanka. The ash sample was sieved to obtain uniform particles with a mesh size of 200 µm.
- Waste papers: Collected internally from the university premises. All collected papers were used to prepare the pulp without undergoing any categorization process.
- Water: Distilled water was used instead of tap water to prepare samples to minimize the potential effects of minerals mixed with regular water.

The compositions of each sample are indicated in Table 2.

Table 2. Composition of paper and SCBA.

Sample	Water 90%	Paper		SCBA	
	$((V \pm 0.5) \times 10^{-3}$ L)	Weight $(W \pm 0.01) \times (10^{-3}$ kg)	Percentage (%)	Weight $(W \pm 0.01) \times (10^{-3}$ kg)	Percentage (%)
1	450	47.50	95	2.5.00	5
2	450	45.00	90	5.00	10
3	450	42.50	85	7.50	15
4	450	40.00	80	10.00	20
5	450	37.50	75	12.50	25

Even though the sample sizes are different, the paper pulp preparation procedure was the same for all cases. Each paper sample was crushed and beaten for 2 min to ensure the uniform conditions of the samples. Soon after crushing, predetermined amounts of SCBA was added to the separate samples, and then repeated beating was carried out for another 1 min. For compression testing, the wet compression molding method was used to

prepare cylindrical samples using a specially designed compression rig under a metered compression load of 2 tons. For tensile testing, bending testing, and biodegradability analysis, thin sheets (Figure 1) were prepared following a conventional wet dipping method.

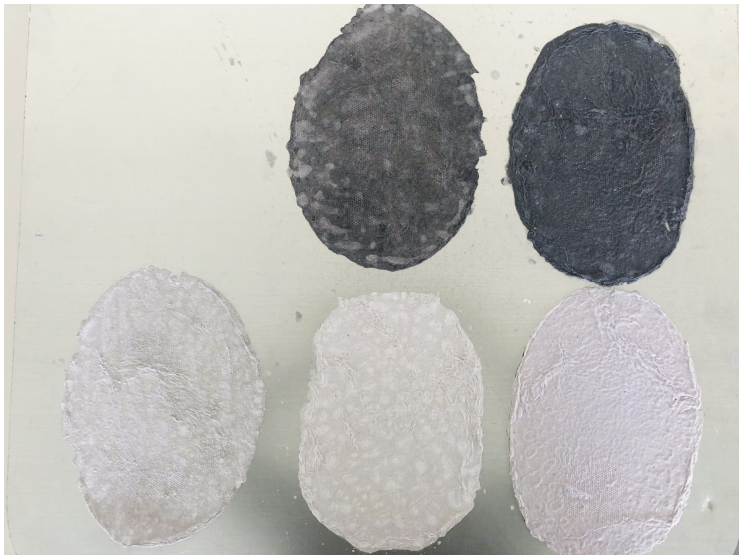


Figure 1. Five fabricated thin sheets using the conventional wet dipping method for tensile testing.

Soon after ejecting, the samples were dried in an electric oven at a temperature of 105 °C for a duration of 48 h. To ensure zero moisture content in the samples, the weight of the samples (Figure 2) was measured intermittently until it showed a constant weight. To enhance the reliability of the results, five replicates were prepared for mechanical testing and ten for degradability analysis, following standard procedures for each.

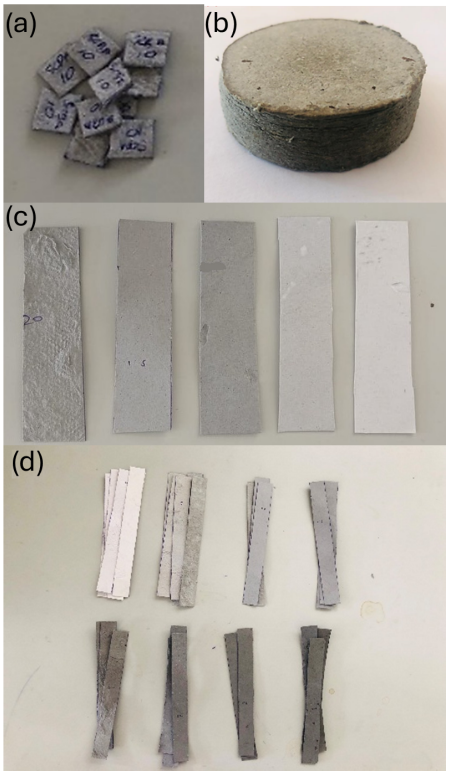


Figure 2. (**a**) Samples for FTIR, XRD, SEM, and biodegradability tests. (**b**) Sample for compressive strength test. (**c**) Samples for bending test. (**d**) Samples for tensile strength test.

The surface morphology of cellulosic fibers was examined using scanning electron microscopy (SEM) with an accelerating voltage of 15–20 kV. Before examination, a fine layer of gold was sprayed on samples by an ion sputter coater with a low deposition rate. XRD provided diffraction patterns that revealed the crystallinity and phase composition of the cellulose matrix, offering insights into its mechanical strength and degradation behavior. Powder samples (2–4 g) were finely ground to 200 mesh for homogeneity, while thin film samples were affixed with double-sided tape. FTIR identified functional groups and assessed chemical interactions between SCBA and the pulp, providing insights into material compatibility and biodegradability. The samples were oven-dried at 105 °C for 4–5 h, mixed with KBr in a ratio of 1:200 (w/w), and pressed under vacuum to form pellets. The FTIR spectrum of the samples was recorded in the absorbance mode in the range of 500–4000 cm^{-1}.

Cylindrical samples were tested for compressive strength using an NL Scientific 100 kN Universal Testing Machine (UTM) (Figure 3a), and load vs. displacement values were obtained. To analyze the bond strength between layers, it was decided to perform the compression test on an axis perpendicular to the initial vertical compression axis, which was used during wet compression molding. Further, thin sheets of samples were subjected to the tensile test (Figure 3b) and three-point bending test (Figure 3c). These tests were conducted using WDW-0.1E UTM, made by Times Group China, which has a 100 N load range under a 0.001% measuring accuracy.

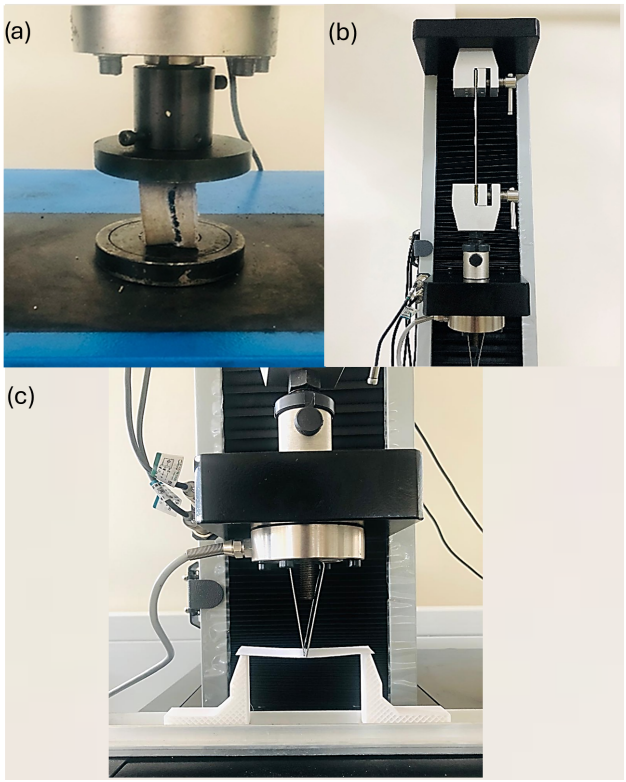


Figure 3. (**a**) Universal Testing Machine (UTM) configured for compressive strength evaluation. (**b**) Apparatus for tensile testing of sheet specimens. (**c**) Setup used for three-point bending test analysis.

The three-point bending test was performed using a standard setup, where the specimen was supported at both ends and loaded at the center to evaluate its flexural behavior (Figure 4).

The tensile and bending tests were conducted according to the relevant ASTM and ISO standards.

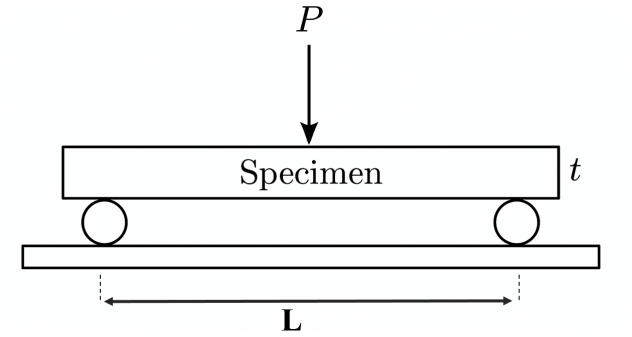


Figure 4. Three-point bending setup showing applied force (P), specimen, span length (L), and thickness (t).

Sample dimensions and test parameters for mechanical testing are presented in Table 3, following the relevant standards.

Table 3. Sample dimensions and test parameters for mechanical testing.

Parameter	Tensile Strength Test (ASTM D828)	Flexural Strength Test (ISO 5628: 2012)
Sample length	250 mm (Gauge length: 180 mm)	Total length: 80 mm (support span: 70 mm)
Sample width	25 mm (±0.1 mm)	25 mm (±0.1 mm)
Sample Thickness	1 mm	0.8 mm
Test speed	20 mm/min (±5 mm/min)	5 mm/min
Reference	[19]	[20]

As one of the main objectives of this research study was to enhance the biodegradability of the samples while maintaining the required mechanical properties, a proper analysis of the level of biodegradability with the addition of SCBA was crucial. As suggested by SFS EN14046 [21], thin-sheet samples were buried in an artificial indoor pit under controlled conditions. Accordingly, the weights of the samples were measured and averaged at 20 days, 60 days, and 90 days. To enhance the accuracy of results, it was decided to place 10 pieces of the same composition and consider the average value (Figure 5).



Figure 5. Experimental setup for biodegradation testing, showing soil-filled compartments with test samples arranged systematically for analysis.

To ensure consistency in biodegradation conditions, the artificial soil used in the indoor pit was composed of a controlled mixture of topsoil, compost, and sand in a 2:1:1 ratio, which was homogenized to maintain a stable and reproducible microbial composition across all test cycles. The experimental environment was maintained at a constant room

temperature of 27 ± 1 °C with relative humidity around 65%, simulating moderate ambient conditions. Weekly moisture content was sustained by spraying 100 mL of deionized water uniformly across the pit surface. The percentage of biodegradation was evaluated based on the weight loss method using the formula

$$\text{Weight loss (\%)} = \left(\frac{W_0 - W_t}{W_0}\right) \times 100 \quad (1)$$

where W_0 is the initial dry weight, and W_t is the dry weight after time t (20, 60, or 90 days). These additions ensured that both microbial activity and moisture levels were adequately controlled, allowing for a more accurate assessment of the effect of SCBA on the biodegradability of the composite samples.

3. Results

3.1. Characterization

XRD analysis was conducted to obtain diffraction patterns, which were used to assess the degree of crystallinity and identify the phase composition of the material.

Figure 6 reveals dominant crystalline phases such as Quartz (Q), Cristobalite (C), and Hematite (Fe_2O_3) (Fe). The presence of these peaks suggests a complex mineral composition, likely formed under high-temperature conditions (700–800 °C). Notably, silicate phases such as Quartz and Cristobalite, both polymorphs of SiO_2, play distinct roles in the performance of ash-reinforced packaging materials. Quartz, being largely inert, may act as a micro-filler that enhances structural packing and improves dimensional stability [8]. Cristobalite, depending on its degree of crystallinity and surface activity, could contribute to thermal resistance and barrier properties by limiting molecular diffusion through the matrix [8]. Although Hematite is not chemically reactive in typical polymer matrices, it can influence thermal reflectivity, opacity, and UV shielding properties important for packaging applications [22].

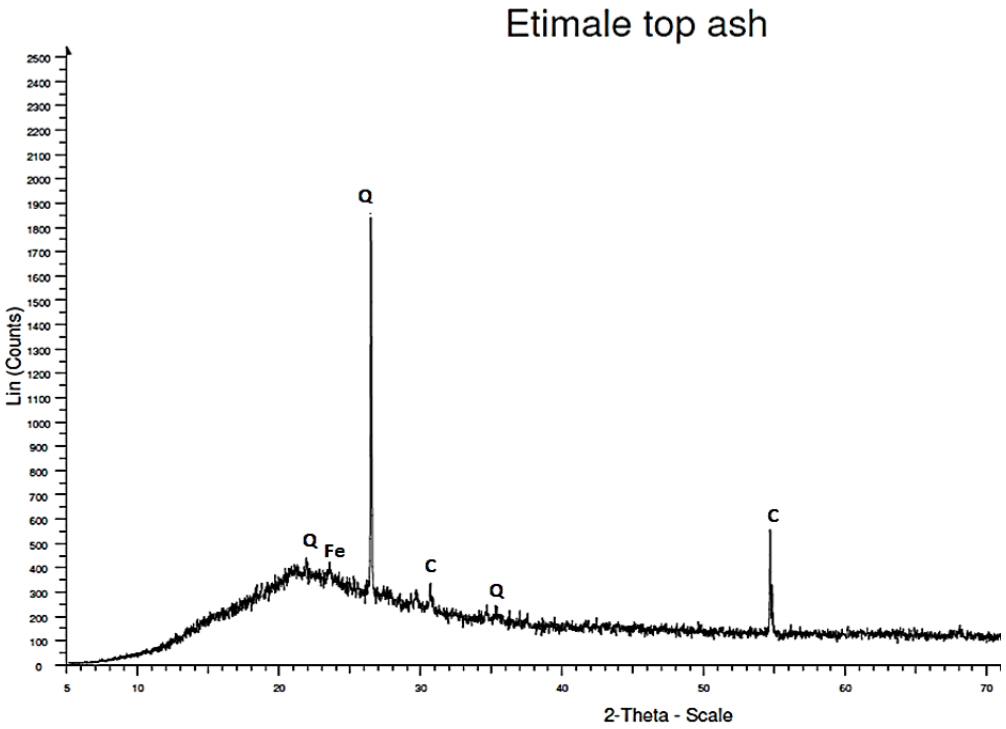


Figure 6. The XRD pattern of Ethimale top ash. Q = Quartz, C = Cristobalite, Fe = Hematite (Fe_2O_3).

Figure 7 presents the SEM image of Ethimale top ash. The particle size distribution of Ethimale top ash exhibited a broad range, with D10, D50, and D90 values of 8.37 ± 0.25 µm, 46.71 ± 2.49 µm, and 117.43 ± 14.86 µm, respectively. The terms D_{10}, D_{50}, and D_{90} refer to specific percentiles in the particle size distribution based on the cumulative volume (or mass) distribution:

- D_{10}: The particle diameter at which 10% of the sample's total volume consists of smaller particles.
- D_{50}: The median particle diameter, meaning 50% of the particles are smaller than this size.
- D_{90}: The diameter below which 90% of the sample's particles fall.



Figure 7. The SEM image for Ethimale top ash subjected to burning temperatures ranging from 700° to 800°.

This indicates the presence of both fine and coarse particles, which could influence the material's packing behavior and reactivity. Furthermore, the observed dominance of prismatic particles suggests a higher degree of calcination, indicating effective thermal treatment.

The analysis aims to compare samples containing sugarcane bagasse ash (SCBA) with those without SCBA incorporation in order to evaluate the influence of SCBA on the properties, performance, and other relevant characteristics of paper pulp-based materials.

Figure 8 shows the XRD patterns of the composite samples with different concentrations of SCBA. All four lines in the graph show nearly the same positions for peaks, including the paper pulp sample without SCBA. The crystalline structure and degree of crystallinity were assessed to determine the influence of SCBA on the cellulose matrix. A shift in diffraction peaks was observed with increasing SCBA content, suggesting a disruption in crystalline order. Specifically, a primary cellulose peak near 22.5° shifted slightly toward higher angles, indicating a reduction in interplanar spacing (d-spacing), as calculated using Bragg's law ($n\lambda = 2d \sin\theta$) (Table 4).

Table 4. Main diffraction peak position and calculated interplanar spacing (d-spacing) based on Bragg's law.

SCBA Content (%)	2θ (°)	d-Spacing (nm)
0%	22.5	0.394
5%	22.8	0.389
10%	23.1	0.385
15%	23.3	0.381

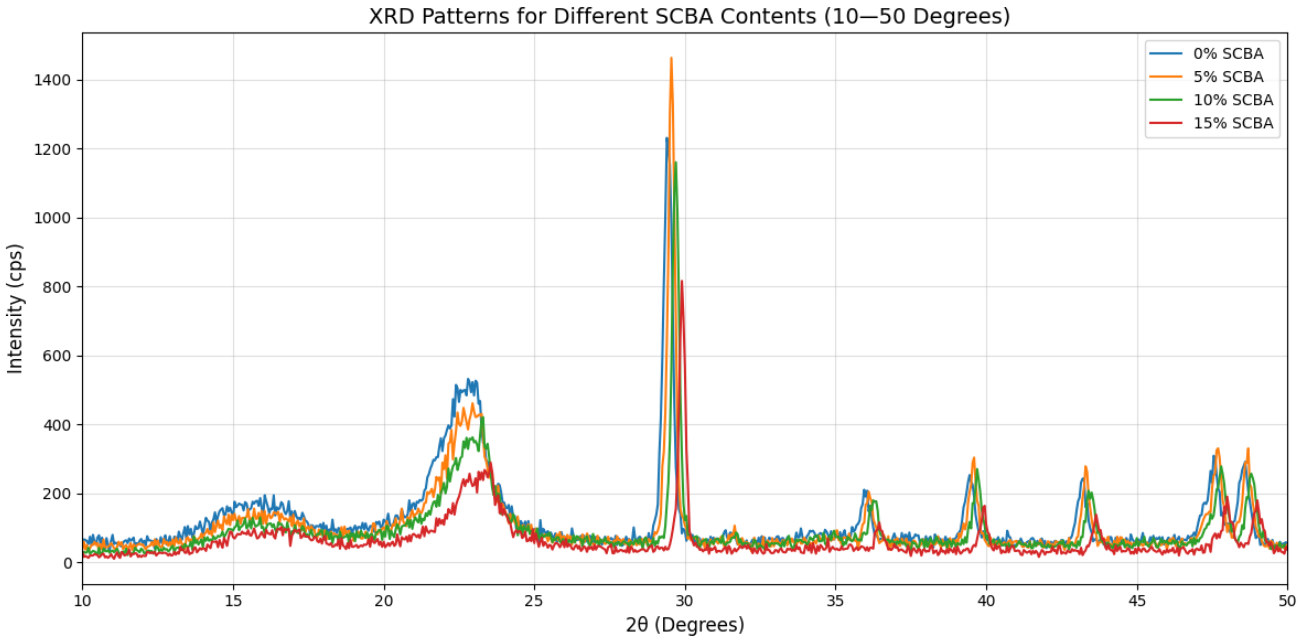


Figure 8. XRD of paper pulp samples with different SCBA contents.

The calculated d-spacing, as in Table 4, decreased from 0.394 nm in 0% SCBA to 0.381 nm in the 15% SCBA sample, reflecting a slight reduction in the crystalline order. Miller indices corresponding to the (002) planes confirmed the dominance of the cellulose structure [23,24]. This suggests a decrease in the degree of crystallinity within the pulp matrix, which is known to significantly affect mechanical behavior in biocomposites [25]. Cellulose crystallinity plays a key role in determining rigidity, tensile strength, and resistance to deformation due to the highly ordered hydrogen bonding network within its crystalline domains [26]. The observed reduction in crystallinity correlates with weaker intermolecular interactions and potentially less efficient load transfer between the pulp matrix and SCBA filler [25]. Furthermore, the amorphous components present in SCBA may act as physical barriers during cellulose microfibril formation, contributing to the disruption of crystalline regions [27]. While low SCBA concentrations may enhance flexibility by acting as spacers or plasticizers, excessive loading appears to impair the structural continuity necessary for effective stress distribution [17].

SEM was used to analyze the surface morphology and fiber distribution of the SCBA-reinforced pulp composites. Images showing surface morphologies of the cellulose fibers and nanocrystals were taken.

Images (Figure 9) revealed that the surface of the control (0% SCBA) composite appeared relatively compact and smooth, whereas composites with 10% and 15% SCBA exhibited increased surface roughness and microvoids. No significant fiber separation was evident in the 15% SCBA sample; instead, SCBA particles appeared embedded within the fiber matrix. These observations indicate partial filler dispersion rather than significant structural reorganization. The visual difference between formulations was subtle; however, a higher SCBA content corresponded to increased surface porosity, potentially enhancing water absorption and biodegradability.

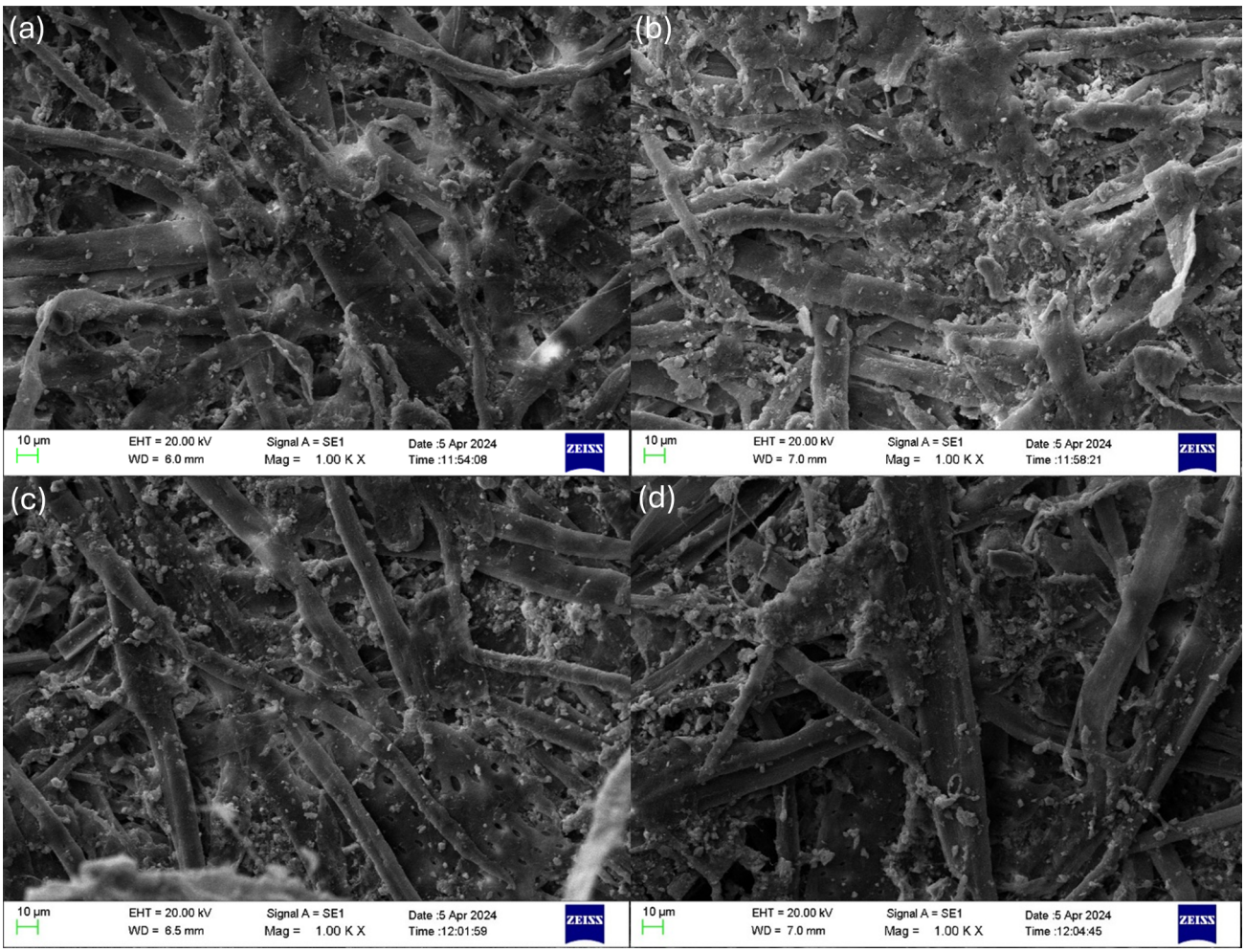


Figure 9. SEMimages of samples with varying SCBA content. (**a**) SCBA content 0%. (**b**) SCBA content 5%. (**c**) SCBA content 10%. (**d**) SCBA content 15%.

FTIR is a fascinating technique to evaluate structural variations in samples due to chemical treatments and also the identification of functional groups, polymer interactions, and possible chemical modifications.

FTIR spectroscopy was used to investigate the structural and compositional changes in paper samples with different percentages of SCBA incorporation (Figure 10). The sample (0% SCBA) indicates the pure paper pulp without any SCBA addition; the characteristic FTIR pattern of cellulose and hemicellulose fibers in the paper pulp sample is shown in Table 5.

The FTIR spectra of the samples reveal distinct absorption bands corresponding to both inorganic and organic components. Peaks in the 400–850 cm^{-1} region are characteristic of silica-based materials. The absorption bands between 1030 and 1750 cm^{-1} correspond to vibrational modes of the organic matrix, including cellulose, hemicellulose, and lignin. These peaks reflect functional groups involved in the structural framework of the pulp. Additionally, prominent peaks above 2900 cm^{-1} are attributed to C–H stretching vibrations, typical of polysaccharides and lignin, indicating the retention of organic components despite SCBA incorporation.

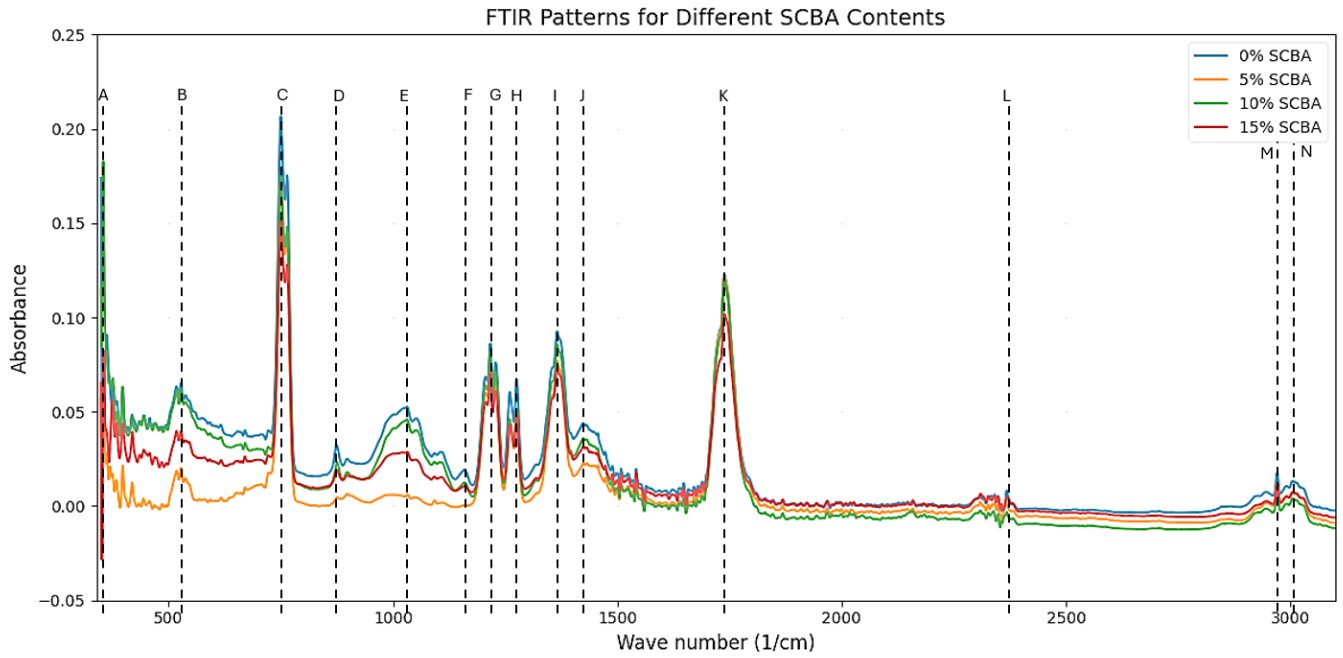


Figure 10. FTIR of samples with SCBA content (0–15%).

As SCBA content increases, peak intensities show a non-linear trend. The 5% SCBA sample exhibits a general reduction in key absorption bands relative to pure pulp, suggesting initial disruption of hydrogen bonding within the cellulose network [28]. However, at 10% SCBA loading, certain features—particularly in the 1030–1150 cm^{-1} region—partially recover before declining again at 15% SCBA. These changes likely reflect modifications in the pulp's supramolecular organization influenced by SCBA-induced interactions such as hydrogen bonding, steric effects, or silanol incorporation [26,28].

Table 5. FTIR peak assignments for SCBA-modified and control pulp samples.

Label	Wavenumber (cm^{-1})	Assignment	References
A	400–430	Si–O rocking vibration (SCBA silica)	[28–30]
B	500–550	Si–O bending modes (SCBA)	[28–30]
C	740–760	Si–O–Si symmetric stretching (Siloxane network)	[29,30]
D	840–860	Si–O rocking vibration (Amorphous silica)	[29,30]
E	1025–1040	C–O stretching (alcohols, ethers, polysaccharides) (Cellulose, hemicellulose)	[24,26,31]
F	1160–1180	C–O–C asymmetric stretching (glycosidic linkage) (Cellulose)	[24,26,31]
G	1215–1230	C–O stretching (aromatic ethers) (Lignin, hemicellulose)	[24,26,31]
H	1250–1265	C–O–C bridge/ether vibrations (Lignin)	[24,26,31]
I	1350–1370	CH_3 bending/COO^- symmetric stretch (Cellulose, hemicellulose)	[24,26,31]
J	1420–1440	CH_2 bending/O–H bending (Cellulose, lignin)	[24,26,31]
K	1720–1750	C=O stretching (ester, carboxyl) (Hemicellulose, lignin)	[24,26,31]
M	2920–2950	C–H asymmetric stretching (CH_2 groups) (Cellulose, lignin)	[24,26,31]
N	2990–3010	Aromatic/aliphatic C–H stretching (Lignin)	[24,26,31]

The decreased absorbance in the O–H and C–H bending (1430–1460 cm^{-1}) regions implies fewer accessible hydroxyl and aliphatic groups, potentially due to stronger intermolecular bonding or partial substitution by SCBA mineral phases [27–29]. Meanwhile, the increased absorbance at 10% SCBA in the C–O–C and Si–O–Si stretching bands (1030–1150 cm^{-1}) suggests the formation of intermolecular linkages, possibly via hydrogen bonding or siloxane bridging between cellulose and silanol-containing SCBA particles [28,32]. This supports beneficial restructuring where moderate SCBA additions reinforce the hydrogen bonding network and enhance pulp matrix integrity.

Above 1500 cm^{-1}, the reduced intensity in C=O and O–H bending regions (1640–1750 cm^{-1}) may result from decreased functional group mobility due to chemical masking, restricted chain motion, or physical encapsulation by amorphous silica [29,33]. These spectral shifts indicate evolving chemical interactions within the matrix, transitioning from a purely hydrogen-bonded biopolymer to a composite framework incorporating silica-mediated interactions and a possible shift in crystallinity versus amorphous content [24,26,28].

The 0% SCBA sample showed higher FTIR absorbance in regions related to hydroxyl, carbonyl, and ether groups due to more free functional groups in the pure pulp matrix. Adding SCBA introduces amorphous silica and ash components that interact with these groups, reducing their availability and infrared activity. Additionally, silica can cause spectral overlap and scattering, further lowering absorbance. Thus, SCBA alters the pulp's supramolecular structure, leading to lower or shifted FTIR intensities compared to the unfilled pulp [34–37].

Together, these spectral features suggest the integration of SCBA minerals within the organic pulp matrix, potentially influencing the composite's mechanical properties.

3.2. Compression Test

Since specimens show ductile properties, it was difficult to identify a sudden failure. Therefore, it was decided to compare the stress–strain plots of each sample. As per the compressive stress vs. strain behavior (Figure 11), all SCBA-added samples showed significant compressive property enhancement compared to the base sample, which was prepared using pure paper. Additionally, the sample with 15% SCBA showed the maximum compressive strength (2.51 MPa) among other samples, which was approximately a 13% enhancement in compressive properties compared to the pure paper-based sample. When considering the ultimate compressive strength values of 15–20% samples, we confirmed that further addition of SCBA leads to a reduction in compressive properties.

3.3. Tensile Test

Through the tensile tests, tensile load (N) vs. displacement of samples (mm) was obtained for each composition. Accordingly, stress (MPa) and strain values for each data point were calculated, incorporating the sample's average thickness (mm) and length (mm).

Similarly, there was a positive effect on tensile properties by adding SCBA to the pulp samples since the samples with 5–10% showed a significantly higher ultimate tensile stress compared to the pure paper pulp-based samples. Among them, the sample with 5% SCBA showed a maximum strength of 3.0 MPa (approx.), which was 20% higher than the base sample. Accordingly, the calculated Young's modulus of the 5% SCBA-added sample, which was 310.12 MPa, was 7% higher than the base sample. In addition to that, the SCBA-mixed samples showed good elastic/cushioning properties, where maximum deflection was significantly higher than the base sample (Figure 12). Furthermore, based on the stress values of 15% and 20% SCBA-contained samples, increased SCBA amounts led to a reduction in tensile properties.

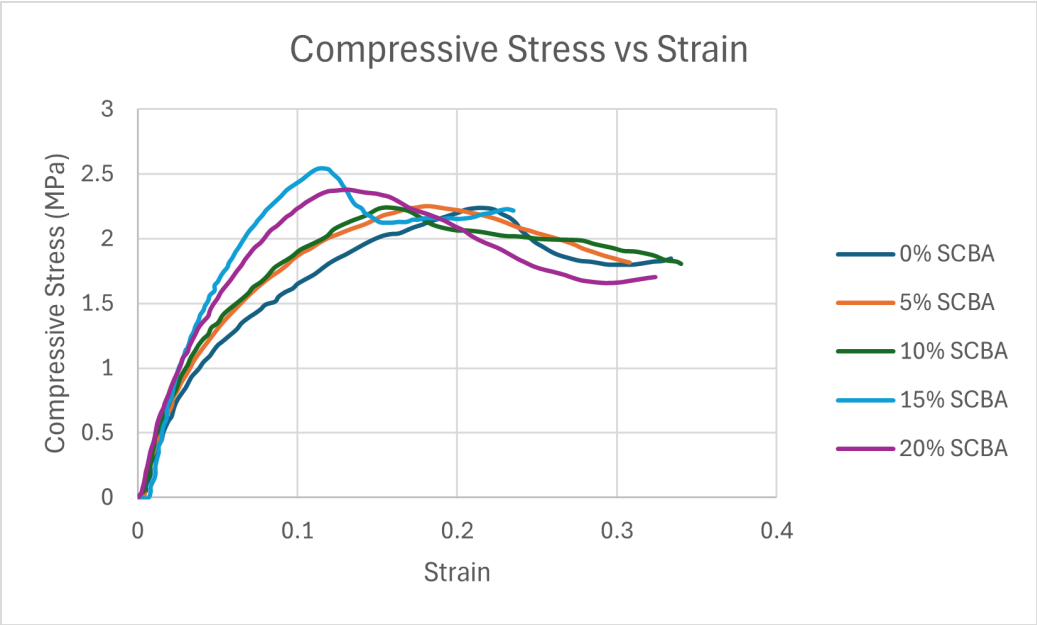


Figure 11. Stress vs. strain for compression test: One-way ANOVA analysis ($p = 0.0041$) based on five replicates indicates a statistically significant effect of SCBA content on the measured values, with a peak observed around 15% SCBA.

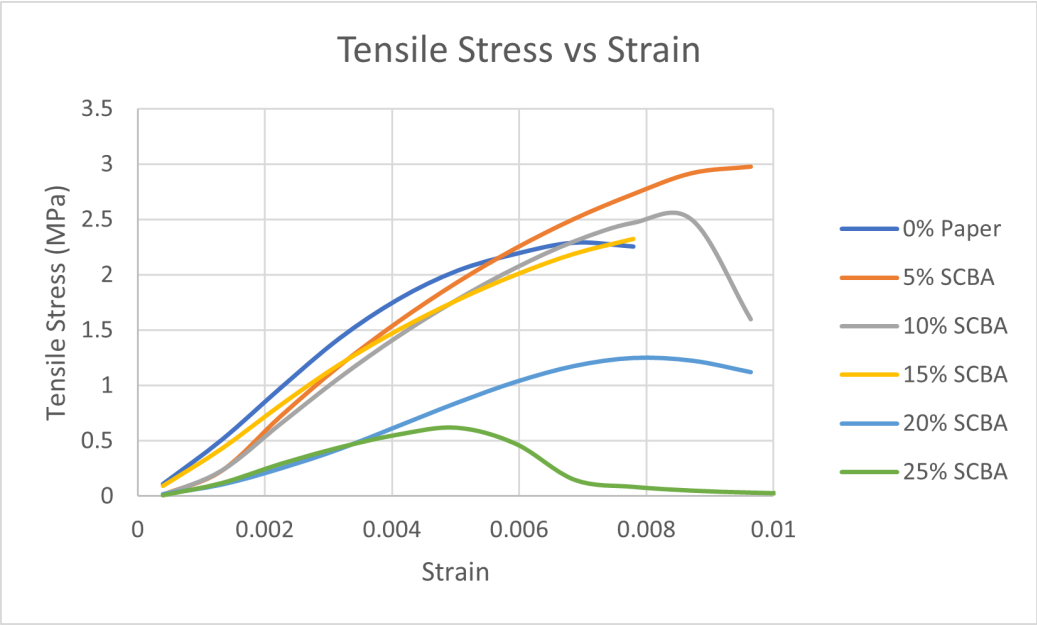


Figure 12. Tensile stress vs strain graph for samples with 0–25 % SCBA.

In the graph (Figure 13), the mean ultimate tensile strength (UTS) of the SCBA samples is shown, with error bars indicating the standard deviation from five replicates. Furthermore, there is a statistically significant effect of SCBA content on the measured values ($p = 3.84 \times 10^{-9}$), with values peaking around 5% SCBA.

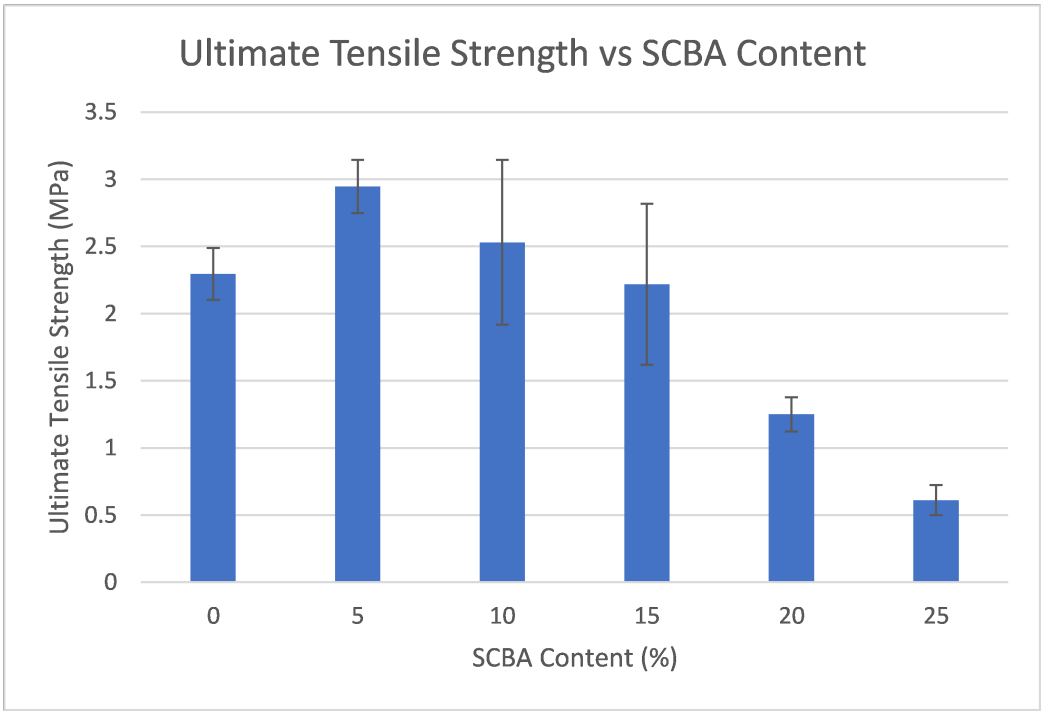


Figure 13. Variation of ultimate tensile strength with different SCBA content levels.

3.4. Bending Test

The bending load (P) vs. deflection data obtained through the three-point bending test were subjected to fundamental calculations to calculate the maximum bending stress (σ_{max}) on the specimen, considering the thickness (t).

$$\sigma_{max} = \frac{3PL}{bt^2} \tag{2}$$

where

- P: applied bending load,
- L: supported length,
- b: specimen width,
- t: specimen thickness.

The graph (Figure 14) indicates that the sample with 5% SCBA exhibits superior flexural properties compared to the rest of the samples. In comparison to the base sample, the 5% SCBA-mixed samples show an approximate 25% enhancement in bending strength compared to the pure pulp-based sample. Furthermore, the highest flexural stiffness is recorded as $p = 3.31 \times 10^{-4}$ Nm^2, which is a 7% enhancement compared to the base sample. The further SCBA addition led to a reduction in flexural properties. Since bending strength depends on both compressive and tensile strengths, pulp-based hose results cumulatively affected the overall bending strength.

3.5. Degradability Analysis

The biodegradability analysis was performed based on both visual inspection and weight-based analysis.

With the increase in SCBA content in the buried samples, sample weights were significantly reduced over time (Figure 15). In accordance with the obtained weight loss percentage values of samples, the SCBA-added sample showed superior biodegradability compared to the pure paper-based samples (Figure 16).

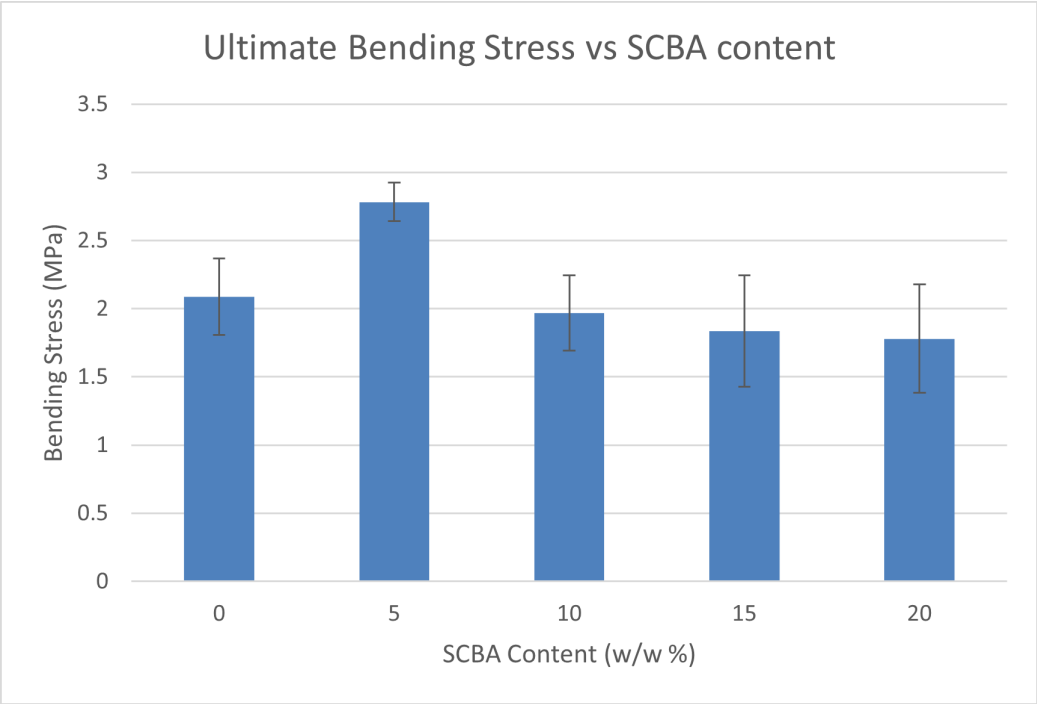


Figure 14. Ultimate bending stress vs. SCBA content for the bending test: One-way ANOVA analysis ($p = 4.35 \times 10^{-4}$) based on ten replicates, indicating a statistically significant effect of SCBA content on the measured values, with a peak observed at around 5% SCBA.

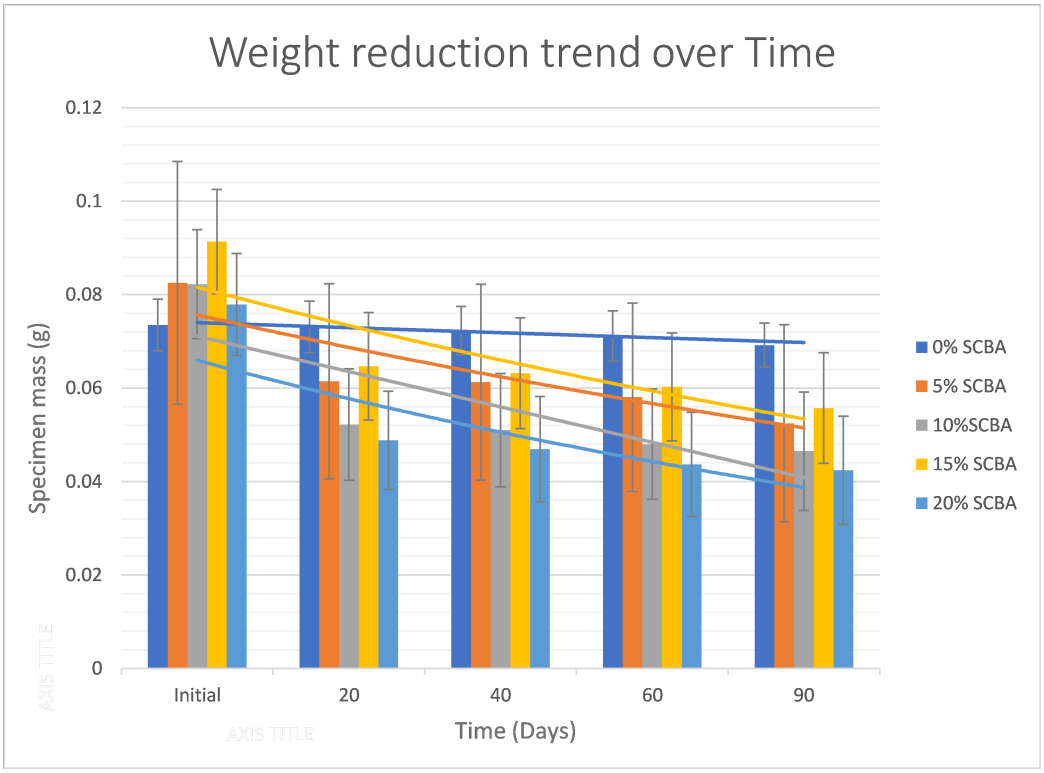


Figure 15. Weight reduction trend over number of days.

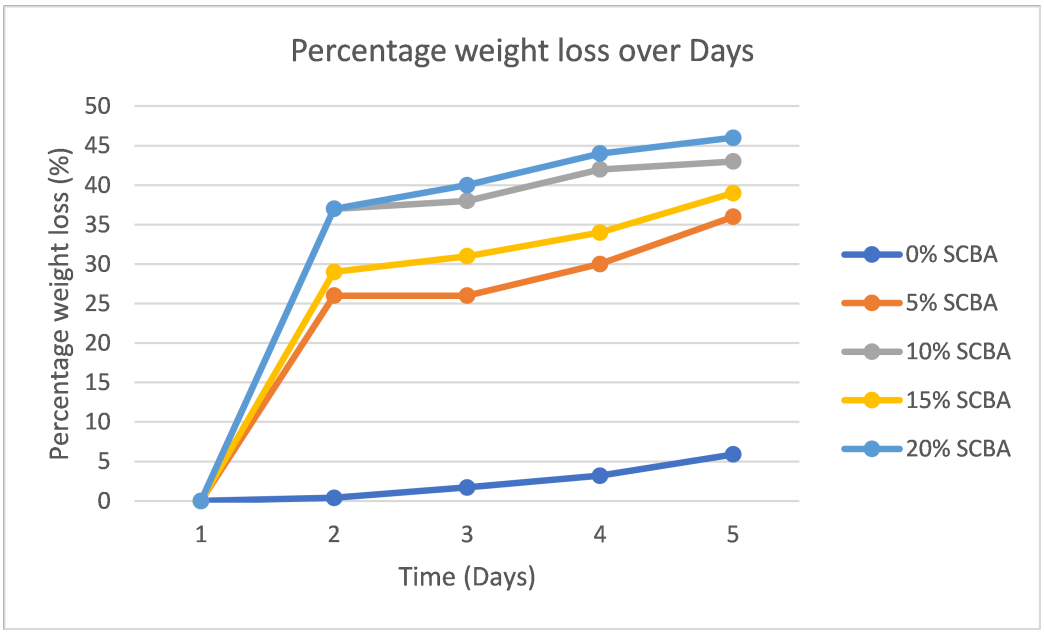


Figure 16. Weight loss percentage over time.

According to Table 6, the results clearly indicate that samples incorporating higher percentages of sugarcane bagasse ash (SCBA) display significant visual signs of increased biodegradability. This trend suggests a positive correlation between SCBA content and the extent of degradation observed. Among the tested samples, the one containing 20% SCBA exhibited the most substantial degradation, highlighting its superior performance in terms of biodegradability.

Table 6. Visual appearance of samples with varying SCBA contents over 90 days.

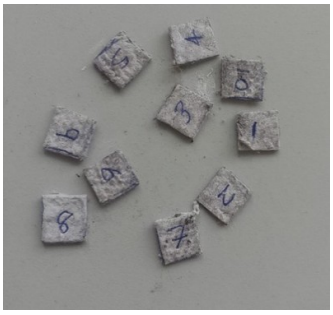
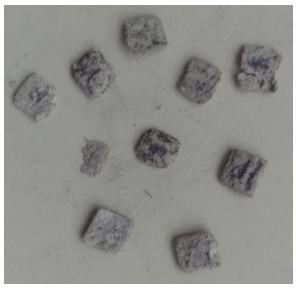
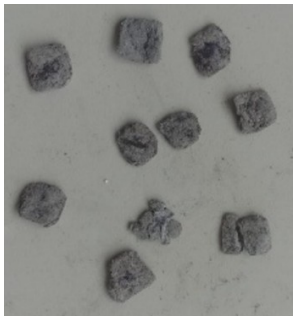
Composition	Initial Appearance	After 90 Days
Pulp paper-based		
5% SCBA		

Table 6. *Cont.*

Composition	Initial Appearance	After 90 Days
10% SCBA		
15% SCBA		
20% SCBA		

4. Conclusions

This study confirms the strong potential of biodegradable pulp-based materials as sustainable alternatives for packaging, combining structural reliability with environmental compatibility.

- Optimal Integration: SEM analysis indicated that 10–15% SCBA achieved a well-bonded matrix with minimal defects.
- Chemical Composition: FTIR analysis revealed characteristic bands of cellulose, hemicellulose, and lignin in all samples, along with additional silicate-related peaks in SCBA-modified samples, indicating 10% SCBA effective integration.
- Structural Changes: XRD analysis revealed a shift in peaks toward higher 2θ angles as the SCBA content increased, suggesting a decrease in d-spacing and a denser molecular structure. To preserve an optimal balance between rigidity and flexibility, the SCBA content was appropriately limited to 15%.

When considering the mechanical properties, tensile strength was slightly higher than the compressive strength of all corresponding samples due to the availability of cellulose fibers. It should be especially noted that the trade-off between property values and balancing between biodegradability and mechanical strength was evident. The higher porosity and higher silica contents in the paper pulp material sample enhanced the biodegradability but simultaneously reduced mechanical flexibility, making the composite material hard and brittle. This was noticeable for 15% SCBA, where excessive porosity resulted in a weakened structure with visible fractures.

In conclusion, the following key findings were observed.

- Tensile Properties: The composite containing 5% SCBA exhibited the highest tensile strength, indicating improved fiber–matrix interactions at lower SCBA contents.
- Compressive Properties: The sample with 15% SCBA demonstrated superior compressive strength, suggesting that increased SCBA content enhances the material's resistance to compressive loads.
- Flexural Properties: Flexural strength was found to be highest in the 5% SCBA sample, likely due to optimal dispersion and bonding of the ash particles at this concentration.
- Biodegradability: The biodegradability of the composites was found to be directly proportional to the SCBA content. Samples with higher SCBA levels showed greater degradation, highlighting SCBA's potential as an eco-friendly additive for enhancing environmental performance.

Overall, the results indicate that SCBA-modified paper pulp composites show significant potential as eco-friendly, strong packaging materials. However, careful optimization of SCBA content is further necessary to balance sufficient mechanical strength with good barrier properties, such as moisture and thermal resistance.

Author Contributions: Conceptualization, K.R.K. and S.V.A.A.I.; methodology, H.M.D.U.S., S.V.A.A.I., J.D.C., and W.G.C.M.K.; software, H.M.D.U.S.; validation, H.M.D.U.S., and S.V.A.A.I.; formal analysis, S.V.A.A.I., H.V.V.P.; investigation, J.D.C.; resources, H.V.V.P.; data curation, D.K.A.I.; writing—original draft preparation, H.M.D.U.S., S.V.A.A.I., and G.D.C.P.G.; writing—review and editing, G.D.C.P.G., and M.K.D.M.G.; visualization, H.M.D.U.S., and J.D.C.; supervision, K.R.K.; project administration, K.R.K.; funding acquisition, S.V.A.A.I. All authors have read and agreed to the published version of the manuscript.

Funding: Science and Technology Human Resource Development Project, Ministry of Education, Sri Lanka, funded by the Asian Development Bank: CRG R3 SB4.

Data Availability Statement: The original contributions presented in the study are included in the article; further inquiries can be directed to the corresponding author.

Acknowledgments: The authors gratefully acknowledge the support provided by the Research Grant: Competitive Research Grant Round 3, Science and Technology Human Resource Development Project (STHRDP) (Grant No. CRG-R3-SB-4).

Conflicts of Interest: The authors declare no conflicts of interest.

References

1. Song, J.H.; Murphy, R.J.; Narayan, R.; Davies, G.B.H. Biodegradable and compostable alternatives to conventional plastics. *Philos. Trans. R. Soc. B* **2009**, *364*, 2127–2139. [CrossRef] [PubMed]
2. Marsh, K.; Bugusu, B. Food packaging—Roles, materials, and environmental issues. *J. Food Sci.* **2007**, *72*, R39–R55. [CrossRef] [PubMed]
3. Kusuma, H.S.; Permatasari, D.; Umar, W.K.; Sharma, S.K. Sugarcane bagasse as an environmentally friendly composite material to face the sustainable development era. *Biomass Convers. Biorefinery* **2024**, *14*, 26693–26706. [CrossRef]
4. Jamil, T.; Nazli, Z.I.; Habib, F.; Jamil, M.I.; Javed, M. Utilization of cellulose nanofibrils from sugarcane bagasse in biodegradable films. *Sustainability* **2023**, *17*, 4128.
5. Rainey, T.J.; Covey, G. Pulp and Paper Production from Sugarcane Bagasse. In *Biomass and Bioenergy: Processing and Properties*; Wiley: New York, NY, USA, 2016; Chapter 10. [CrossRef]
6. Siracusa, V.; Rocculi, P.; Romani, S.; Dalla Rosa, M. Biodegradable polymers for food packaging: A review. *Trends Food Sci. Technol.* **2008**, *19*, 634–643. [CrossRef]
7. Samanth, M.; Hiremath, P.; Deepak, G.D.; Naik, N.; Arunkumar, H.S.; Heckadka, S.S.; Shivamurthy, R.C. Sustainable Composites from Sugarcane Bagasse Fibers and Bio-Based Epoxy with Insights into Wear Performance, Thermal Stability, and Machine Learning Predictive Modeling. *J. Compos. Sci.* **2025**, *9*, 124. [CrossRef]
8. Rodríguez-Díaz, J.M.; Prieto García, J.O.; Bravo Sánchez, L.R.; da Silva, M.G.C.; da Silva, V.L.; Arteaga-Pérez, L.E. Comprehensive characterization of sugarcane bagasse ash for its use as an adsorbent. *J. Environ. Chem. Eng.* **2021**, *9*, 106358. [CrossRef]

9. Kulasooriya, W.G.C.M.; Sewwandi, H.M.D.U.; Vithanage, V.; Induranga, A.; Kumara, B.S.; Koswattage, K. Experimental analysis of mechanical property enhancement of paper-pulp-based packaging materials using biodegradable additives. *Sustainability* **2024**, *16*, 10310. [CrossRef]
10. Amaraweera, S.M.; Gunathilake, C.; Gunawardene, O.H.; Dassanayake, R.S.; Fernando, N.M.L.; Wanninayaka, D.B.; Rajapaksha, S.M.; Manamperi, A.; Gangoda, M.; Manchanda, A.; et al. Preparation and characterization of dual-modified cassava starch-based biodegradable foams for sustainable packaging applications. *ACS Omega* **2022**, *7*, 19579–19590. [CrossRef]
11. Ediyilyam, S.; George, B.; Shankar, S.S.; Dennis, T.T.; Wacławek, S.; Černík, M.; Padil, V.V.T. Chitosan/Gelatin/Silver Nanoparticles Composites Films for Biodegradable Food Packaging Applications. *Polymers* **2021**, *13*, 1680. [CrossRef]
12. Reshmy, R.; Madhavan, A.; Philip, E.; Paula, S.A.; Sindhu, R.; Binod, P.; Pugazhendhi, A.; Sirohi, R.; Pandey, A. Sugarcane Bagasse-Derived Nanocellulose Reinforced with Frankincense (*Boswellia serrata*): Physicochemical Properties, Biodegradability, and Antimicrobial Effect for Controlling Microbial Growth for Food Packaging Applications. *J. Appl. Polym. Sci.* **2024**, *141*, 52298. [CrossRef]
13. Rukmanikrishnan, B.; Jo, C.; Chae, J.; Kim, S.S.; Lee, J. Stretchable Composite Films Are Prepared by Using Cellulose Pulp with Differential Substitution of Carboxymethyl Cellulose and Thymol with an Infrared Heating Process for Packaging Application. *J. Appl. Polym. Sci.* **2024**, *141*, 52299. [CrossRef] [PubMed]
14. Jo, C.; Kim, S.S.; Rukmanikrishnan, B.; Ramalingam, S.; DS, P.; Lee, J. Properties of Cellulose Pulp and Polyurethane Composite Films Fabricated with Curcumin by Using NMMO Ionic Liquid. *J. Appl. Polym. Sci.* **2024**, *141*, 52300. [CrossRef] [PubMed]
15. Yuvaraj, S.; Rajeswari, N. Preparation of Low-Density Polyethylene (LDPE)/Modified Banana Epidermis Starch (MBES) Based Biodegradable Films and Their Study for Its Suitability in Food Packaging Applications. *J. Appl. Polym. Sci.* **2024**, *141*, 52301. [CrossRef]
16. Kumar, A.; Gupta, V.; Singh, S.; Saini, S.; Gaikwad, K.K. Pine Needles Lignocellulosic Ethylene Scavenging Paper Impregnated with Nanozeolite for Active Packaging Applications. *J. Appl. Polym. Sci.* **2024**, *141*, 52302. [CrossRef]
17. Li, T.; Zhou, Y.; Wu, Q.; Lei, H.; Zhang, Q.; Ren, S. Effects of Lignin Content on the Structure and Properties of Cellulose-Lignin Composites. *Ind. Crops Prod.* **2020**, *154*, 112572.
18. Gupta, B.; Revagade, N.; Hilborn, J. Poly(Lactic Acid) Fiber: An Overview of Its Production, Properties, and Technological Application. *Polym. Int.* **2007**, *56*, 559–569.
19. *ASTM D828-22*; ASTM International. Standard Test Method for Tensile Properties of Paper and Paperboard Using Constant-Rate-of-Elongation Apparatus. ASTM International: West Conshohocken, PA, USA, 2022. Available online: https://store.astm.org/d0828-22.html (accessed on 1 July 2025).
20. Spiridon, I.; Tanase, C.E. Design, Characterization, and Evaluation of Cellulose-Lignin Biocomposites with Improved Properties. *Cellulose* **2018**, *25*, 331–343. [CrossRef]
21. Aryal, R. Utilization of Sugarcane Bagasse for Production of Value-Added Products. Bachelor's Thesis, Centria University of Applied Sciences, Kokkola, Finland, 2019. Available online: https://www.theseus.fi/bitstream/handle/10024/168918/Aryal_Rabin.pdf?sequence=3 (accessed on 1 July 2025).
22. Xu, Y.; Liu, X.; Jiang, Q.; Yu, D.; Xu, Y.; Wang, B.; Xia, W. Development and properties of bacterial cellulose, curcumin, and chitosan composite biodegradable films for active packaging materials. *Carbohydr. Polym.* **2021**, 260, 117778. [CrossRef] [PubMed]
23. French, A.D. Idealized powder diffraction patterns for cellulose polymorphs. *Cellulose* **2014**, *21*, 885–896. [CrossRef]
24. Park, S.; Baker, J.O.; Himmel, M.E.; Parilla, P.A.; Johnson, D.K. Cellulose crystallinity index: Measurement techniques and their impact on interpreting cellulase performance. *Biotechnol. Biofuels* **2010**, *3*, 10. [CrossRef] [PubMed]
25. Moon, R.J.; Martini, A.; Nairn, J.; Simonsen, J.; Youngblood, J. Cellulose Nanomaterials Review: Structure, Properties and Nanocomposites. *Chem. Soc. Rev.* **2011**, *40*, 3944–3993. [CrossRef] [PubMed]
26. Nelson, M.L.; O'Connor, R.T. Relation of certain infrared bands to cellulose crystallinity and crystal lattice type. Part I. Spectra of lattice types I, II, III and of amorphous cellulose. *J. Appl. Polym. Sci.* **1964**, *8*, 1311–1324. [CrossRef]
27. Sun, R.C.; Tomkinson, J.; Ma, P.L. Characterization of lignins from wheat straw by FT-IR spectroscopy. *J. Appl. Polym. Sci.* **2000**, *77*, 638–647.
28. Kondo, T.; Sawatari, C. A Fourier transform infrared spectroscopic analysis of the character of hydrogen bonds in cellulose. *Polymer* **1996**, *37*, 393–399. [CrossRef]
29. Nandiyanto, A.B.D.; Oktiani, R.; Ragadhita, R. How to Read and Interpret FTIR Spectroscopy of Organic Material. *Indones. J. Sci. Technol.* **2020**, *5*, 97–118.
30. Zhang, Y.; Liu, W.; Wang, S.; Li, C. Mechanical and Thermal Properties of Starch-Based Composites Reinforced with Modified Cellulose Fibers. *Polym. Test.* **2019**, *80*, 106089.
31. Ciolacu, D.; Ciolacu, F.; Popa, V.I. Amorphous Cellulose—Structure and Characterization. *Cellul. Chem. Technol.* **2011**, *45*, 13–21.
32. Hubbe, M.A.; Rojas, O.J.; Lucia, L.A.; Sain, M. Cellulosic Nanocomposites: A Review. *BioResources* **2008**, *3*, 929–980.
33. Shingel, K.I. Determination of Structural Peculiarities of Dextran, Pullulan, and γ-Irradiated Pullulan by Fourier-Transform IR Spectroscopy. *Carbohydr. Res.* **2002**, *337*, 1445–1451. [CrossRef]

34. Kumar, A.P.; Singh, J.; Singh, N. Effect of Filler Loading on Mechanical and Morphological Properties of Bagasse Fiber-Reinforced Composite. *J. Reinf. Plast. Compos.* **2009**, *28*, 687–701.]
35. Shen, X.; Liu, C.; Li, X.; Yue, Y.; Wu, Q.; Gao, Y. Effect of Lignin as a Natural Plasticizer on the Hydrogen Bonding Network, Thermal–Mechanical Properties, and Free Volume of Cellulose Films. *Carbohydr. Polym.* **2018**, *195*, 368–376. [CrossRef]
36. Iftiquar, S.M. Structural Studies on Semiconducting Hydrogenated Amorphous Silicon Oxide Films. *arXiv* **2003**, arXiv:cond-mat/0305636. [CrossRef]
37. Faruk, O.; Bledzki, A.K.; Fink, H.P.; Sain, M. Biocomposites Reinforced with Natural Fibers: 2008–2011. *Prog. Polym. Sci.* **2012**, *37*, 1552–1596. [CrossRef]

Disclaimer/Publisher's Note: The statements, opinions and data contained in all publications are solely those of the individual author(s) and contributor(s) and not of MDPI and/or the editor(s). MDPI and/or the editor(s) disclaim responsibility for any injury to people or property resulting from any ideas, methods, instructions or products referred to in the content.